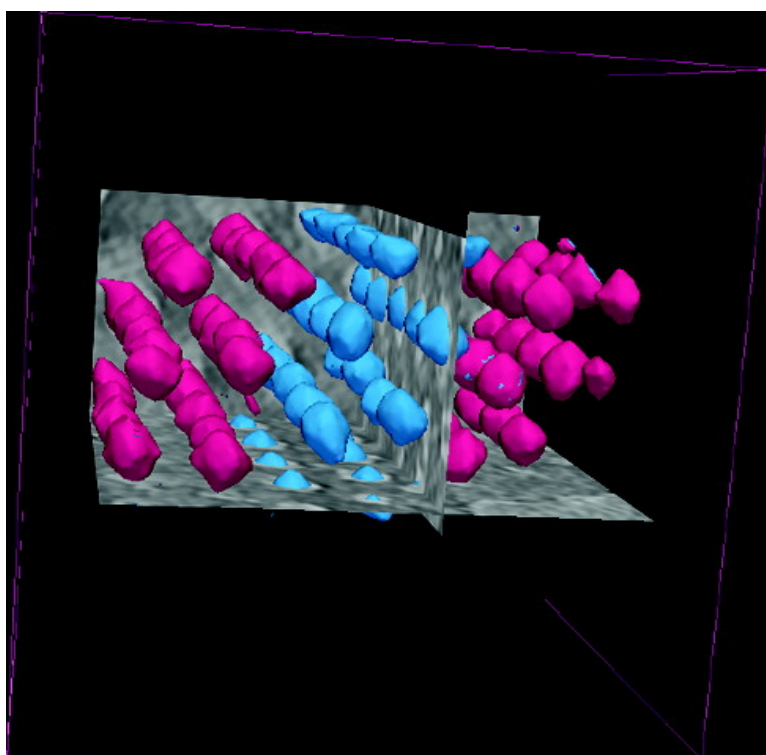Article

Direct Observation of Stacking Faults and Pore Connections in Ordered Cage-Type Mesoporous Silica FDU-12 by Electron Tomography

Ovidiu Ersen, Julien Parmentier, Leonid A. Solovyov, Marc Drillon,
Cuong Pham-Huu, Jacques Werckmann, and Patrick Schultz

More About This Article

Additional resources and features associated with this article are available within the HTML version:

- Supporting Information
- Access to high resolution figures
- Links to articles and content related to this article
- Copyright permission to reproduce figures and/or text from this article

ACS Publications
High quality. High impact.

Direct Observation of Stacking Faults and Pore Connections in Ordered Cage-Type Mesoporous Silica FDU-12 by Electron Tomography

Ovidiu Ersen,*,[†] Julien Parmentier,*,[‡] Leonid A. Solovyov,[§] Marc Drillon,[†] Cuong Pham-Huu,[‖] Jacques Werckmann,[†] and Patrick Schultz[⊥]

Institut de Physique et Chimie des Matériaux de Strasbourg, UMR 7504 CNRS-ULP, 23 rue de Loess, F-67034 Strasbourg Cedex, France, Laboratoire de Matériaux à Porosité Contrôlée, Ecole Nationale Supérieure de Chimie de Mulhouse, UMR CNRS 7016, Université de Haute Alsace, 3 rue Alfred Werner, F-68093 Mulhouse Cedex, France, Institute of Chemistry and Chemical Technology, K. Marx av. 42, 660049 Krasnoyarsk, Russia, Laboratoire des Matériaux, Surfaces et Procédés pour la Catalyse, UMR 7515 CNRS, ECPM, Université Louis Pasteur, 25 rue Becquerel, F-67087 Strasbourg, France, and Department of Structural Biology and Genomics, Institut de Génétique et de Biologie Moléculaire et Cellulaire, CNRS/INSERM/ULP, 1 rue Laurent Fries, BP10142, 67404 Illkirch, France

Received August 8, 2008; E-mail: ovidiu.ersen@ipcms.u-strasbg.fr; julien.parmentier@uha.fr

Abstract: The porous structure and the periodic array of cavities in ordered mesoporous materials with large, three-dimensionally arranged and interconnected pores is thoroughly described by combining electron tomography, small-angle X-ray diffraction, and nitrogen sorption techniques. We used the ability of the electron tomography to provide local three-dimensional information of a nano-object and compared the results to those of the other characterization techniques which furnish global information. We showed thus that the face-centered cubic (fcc) structure usually assigned to the FDU-12 materials is in fact an intergrowth of cubic and hexagonal close-packing structures. This agrees with small-angle X-ray scattering (SAXS) modeling, but for the first time a direct visualization of these stacking faults was achieved. Three-dimensional transmission electron microscopy (3D-TEM) provides also a direct and unique evidence of peculiar stacking defects ("*z*-shifted [111] areas"), as well as an estimate of their density, which have never been reported elsewhere. In addition, interstitial cavities were also observed, revealing the complex defective structure of this material. A direct observation of the nature of the connecting pores was also achieved for the first time, with a resolution limit of 2 nm. Finally, the characteristics of the porous network evidenced by 3D-TEM are used to explain and validate the results obtained by nitrogen sorption experiments.

1. Introduction

Ordered mesoporous materials (pore size in the range of 2−50 nm according to IUPAC classification) with large, self-organized, and interconnected pores have attracted considerable attention in the past few years due to the wide range of potential applications, especially in areas involving selective tunnel diffusion, immobilization and separation of large molecules or biomolecules, or in catalysis, by grafting of specific elements on wall surface. The nanometric cavities in these solids may further be used as nanoreactors to growth-controlled nanocrystals or as hard templates (or host matrixes) for the synthesis of new mesostructured porous materials, opening the route to new physical and chemical properties.[1,2] In the particular case of mesoporous materials with cagelike structures, as exemplified by FDU-12,[3] the design of the structure by appropriate synthesis is a key issue for applications where the final topology is important. For example, in the process of growing nanocrystalline ordered replicas within mesoporous templates, distortions of the network may affect the connectivity between cavities and accordingly the crystal growth process.[1] Beside the primary pore diameter, another important feature for applications requiring diffusion is the pore entrance size.[3] It plays a very important role when the material is employed in the field of filtration, separation, or catalysis where the gaseous diffusion ability through the material framework is an important parameter which needs to be controlled. Several methods were proposed to tune the mesoporous structure of cagelike materials to the targeted application.[4−7]

[†] Institut de Physique et Chimie des Matériaux de Strasbourg.
[‡] Laboratoire de Matériaux à Porosité Contrôlée.
[§] Institute of Chemistry and Chemical Technology.
[‖] Laboratoire des Matériaux, Surfaces et Procédés pour la Catalyse.
[⊥] Institut de Génétique et de Biologie Moléculaire et Cellulaire.

(1) Yue, W.; Zhu, W. *J. Mater. Chem.* **2007**, *17*, 4947.
(2) Tian, B.; Liu, X.; Solovyov, L. A.; Liu, Z.; Yang, H.; Zhang, Z.; Xie, S.; Zhang, F.; Tu, B.; Yu, C.; Terasaki, O.; Zhao, D. *J. Am. Chem. Soc.* **2004**, *126*, 865.

(3) Fan, J.; Yu, C.; Gao, F.; Lei, J.; Tian, B.; Wang, L.; Luo, Q.; Tu, B.; Zhou, W.; Zhao, D. *Angew. Chem., Int. Ed.* **2003**, *42*, 3146.
(4) Matos, J. R.; Kruk, M.; Mercuri, L. P.; Jaronieck, M.; Zhao, L.; Kamiyama, T.; Terasaki, O.; Pinnavaia, T.; Liu, Y. *J. Am. Chem. Soc.* **2003**, *125*, 821.
(5) Fan, J.; Yu, C.; Lei, J.; Zhang, Q.; Li, T.; Tu, B.; Zhou, W.; Zhao, D. *J. Am. Chem. Soc.* **2005**, *127*, 10794.
(6) Yu, C.; Yu, Y.; Zhao, D. *Chem. Commun.* **2000**, 575.
(7) Kruk, M.; Hui, C. M. *J. Am. Chem. Soc.* **2008**, *130*, 1528.

A comprehensive characterization of three-dimensionally (3D) ordered porous materials requires the use of different analytical techniques. Transmission electron microscopy (TEM) has been widely used for the determination of the structure, symmetry, and lattice parameters of ordered porous materials. Combining TEM analysis and small-angle X-ray scattering (SAXS) studies showed that the FDU-12 mesoporous silica is face-centered cubic (fcc).[3,4] This structure agrees also with the X-ray diffraction (XRD) and electron diffraction (ED) patterns, especially for samples with smaller lattice dimensions for which the diffraction peaks are better resolved. Further, depending on the synthesis conditions, some authors claimed the presence of hexagonal (hcp) intergrowths,[4] while others ruled out this hypothesis.[3]

TEM in traditional imaging mode at small magnification allows, normally, observing highly ordered lattice arrays extending over relatively large domains. The determination of more specific parameters (average pore diameter, entrance size, etc.) needs nitrogen sorption measurements and/or TEM investigations of replicas derived from these structures.[4] The pore diameters are also calculated on the basis of idealized models (developed for cylindrical or spherical shapes) requiring lattice parameters and pore volumes to be determined from SAXS or XRD and nitrogen physisorption experiments, respectively. These investigations thus did not allow obtaining reliable values for the size and density of the pore interconnections.

A recent study of the FDU-12 materials[8] combining high-resolution TEM (HRTEM) images recorded at different angles furnished a more reliable description of chosen particle fragments. In addition, calculated electrostatic potential maps allowed a visualization of the overall pore structure and an estimate of the mean cage diameter, in agreement with nitrogen adsorption experiments. Unfortunately, the values obtained for the cage entrance size are not quite accurate and show only a trend in a relative scale depending on the synthesis conditions. Furthermore, the symmetry assignment made for selected fragments cannot rule out the presence of cubic−hexagonal intergrowths in the whole material.

Despite numerous works reported from complementary techniques (including also some specific methods like NMR,[9] thermogravimetric analysis, etc.), the detailed structure of FDU-12 is not fully established today. In particular, they usually fail to deduce reliable values of the individual pore size and connectivity since the traditional techniques furnish averaged information on the bulk sample though the materials are, generally, quite inhomogeneous. Likewise, the stacking defects in the structure are characterized indirectly, e.g., from the diffuse streaks on the ED patterns[10] or by SAXS modeling. Their analysis is important since they influence the properties of the material and those of the templated crystalline replicas.

The classical TEM gives a general view of the structure of the whole system, but it does not allow the determination of accurate parameters of individual pores and their connectivity within the matrix, since the recorded image is an integral projection of the object. The fine structure of a 3D object is lost in the projection, where it is difficult to separate and localize particular characteristics of the object (here, for example, cavity shape or pore interconnections). The limitations of the standard 2D-TEM technique are overcome in the three-dimensional TEM (3D-TEM) or electron tomography which is rapidly developing now. This technique, primarily used in biology, has attracted a growing interest in the field of materials science[11,12] owing to its facilities of extracting specific 3D characteristics of substances with complex morphology, structure, and self-organization at the nanoscale. Such an interest is further promoted by the implementation of new experimental methods allowing a reduction of the diffraction contrast (unwanted in tomography), as, for example, the image recording in large-angle annular dark-field mode.[13] Similarly to any tomographic technique,[14] it consists in the volume reconstruction of an object from a series of 2D images obtained by tilting the specimen with respect to the electron beam. In most of the studies reported in the literature,[15−17] the 3D-TEM technique was principally used to resolve the 3D positions of some individual parts of the sample under observation as well as the whole morphology of complex objects. Looking at mesostructured materials, the electron tomography is the appropriate technique for studying morphology of individual nano-objects as well as their periodic arrangement.

Herein we report on an accurate and complete analysis of the large-cage mesoporous FDU-12 silica by combining small-angle X-ray diffraction (SAXRD), nitrogen sorption, and electron tomography (3D-TEM) techniques. We show in particular that the 3D-TEM is an essential tool to describe precisely both the cavities of these materials and their interconnectivity. Furthermore, the periodic array of the pores and the presence of stacking defects may be closely investigated. Specific parameters of the porous structure will be compared to the averaged ones determined by SAXRD modeling and physisorption. Such a study gives access to exceptionally detailed data on the structure of these materials at nanoscale, which are of first importance for their subsequence use.

2. Experimental Section

2.1. Synthesis of the FDU-12 Mesoporous Materials. The synthesis of FDU-12 silica was derived from the Fan et al. original work.[5] Briefly, triblock copolymers F127 (0.50 g) and KCl (2.5 g) were completely dissolved into 30 mL of 2 M HCl at 15 °C, and then 1,3,5-trimethylbenzene (0.60 g) was added to the solution and the mixture was stirred for 2 h. Tetraethyl orthosilicate (2.08 g) was then added to the previous solution, and the mixture was stirred for 24 h at 15 °C. The mixture was then heated at 100 °C for 24 h. As-made products were obtained by filtration and dried at room temperature in air. Thereafter, the products were calcined at 550 °C for 5 h in air at a heating rate of 1.5 °C min⁻¹.

2.2. Nitrogen Physisorption Study. Measurements were performed at 77 K on a Tristar (Micromeritics) apparatus. Sample was previously outgased at 90 °C for 2 h and then at 150 °C overnight. The pore size distribution (PSD) was determined using the hybrid density functional theory (DFT) model developed by Quantachrom

(8) Yu, T.; Zhang, H.; Yan, X.; Chen, Z.; Zou, X.; Oleynikov, P.; Zhao, D. *J. Phys. Chem. B* **2006**, *110*, 21467.

(9) Kao, H.-M.; Chang, P.-C.; Wu, J.-D.; Chiang, A. S. T.; Lee, C.-H. *Microporous Mesoporous Mater.* **2006**, *97*, 9.

(10) Sakamoto, Y.; Diaz, I.; Terasaki, O.; Zhao, D. Y.; Perez-Pariente, J.; Kim, J. M.; Stucky, G. D. *J. Phys. Chem. B* **2002**, *106*, 3118.

(11) de Jong, K. P.; Koster, A. J. *ChemPhysChem* **2002**, *3*, 776–780.

(12) Weyland, M. *Top. Catal.* **2002**, *21*, 175–183.

(13) Midgley, P. A.; Weyland, M.; Thomas, J. M.; Johnson, B. F. G. *Chem. Commun.* **2001**, 907.

(14) Mobus, G.; Inkson, B. J. *Mater. Today* **2007**, *10*, 18.

(15) Koster, A. J.; Ziese, U.; Verkleij, A. J.; Janssen, A. H.; de Jong, K. P. *J. Phys. Chem. B* **2000**, *104*, 9368.

(16) Kaneko, K.; Inoke, K.; Freitag, B.; Hungria, A. B.; Midgley, P. A.; Hansen, T. W.; Zhang, J.; Ohara, S.; Adschiri, T. *Nano Lett.* **2007**, *7*, 421.

(17) Ersen, O.; Werckmann, J.; Houlle, M.; Pham-Huu, C.; Ledoux, M.-J. *Nano Lett.* **2007**, *7*, 1898.

Instruments (Quantachrome Autosorb 1.52 software) taking into account a spherical porosity above 5 nm and a tubular one below this limit.[18]

2.3. SAXS Measurements. Low-angle XRD measurements were first performed on a Panalytical X'Pert Pro MPD $\theta/2\theta$ and the diagram was indexed with a cubic symmetry (*Fm3m*). In order to get more information, measurements were carried out on the French CRG beamline D2AM at the European Synchrotron Radiation Facility (ESRF) in Grenoble (France). Details about the experimental setup and about data analysis were given in a previous paper.[19] The wavelength used was $\lambda = 0.0816$ nm ($E = 15.193$ keV).

2.4. TEM and 3D-TEM Analysis. 2D-TEM investigations were performed in bright-field mode on a Topcon microscope operated at 200 kV with a point-to-point resolution of 0.18 nm. Before observation, the samples were ultrasonically dispersed in ethanol and a drop of suspension was subsequently deposited onto a carbon membrane grid.

The acquisition of the tilt series for 3D-TEM analysis was performed in bright-field mode on a F20 TECNAI microscope (FEI company) using the FEI Xplore3D software and a 2048 × 2048 pixels cooled CCD array detector. This automated mode of acquisition allowed varying systematically the tilt angle step by step, to correct for defocusing, to maintain the object under study within the field of view, and to record and store the 2D images. Prior to the acquisition, a drop of a solution containing calibrated gold nanoparticles (5 nm) was deposited on the grid supporting the sample, to be used as fiducial markers for the alignment process of the images which precedes the reconstruction. The tilt angles ranged from −70° to 70°, with an image recorded every 2° between −30° and 30° and every 1° elsewhere, giving a total of 110 images. No apparent irradiation damage was observed on the specimen at the end of the acquisition process with duration of about 40 min. The treatment of aligned images series for reconstruction procedure was performed using the IMOD software from the University of Colorado,[20] which uses the weighted-back projection method to compute the volume of the specimen. With our acquisition parameters and specimen characteristics, the spatial resolution in the tomogram presented in this paper was about 1.5 nm in the directions perpendicular to the electron beam. In the parallel direction, the resolution is worse by an elongation factor of 1.3 due to the limited maximum tilt angle,[12] and consequently we consider that the information limit of the 3D analysis is in the present case about 2 nm. For modeling the computed volume, we finally used a segmentation procedure based on the gray-level intensities of the voxels, followed by 3D display using surface rendering methods. More details on the experimental setup, volume reconstruction, and analysis are given elsewhere.[15,21]

3. Structural and Morphological Characterization of FDU-12

3.1. Classical TEM Analysis and SAXRD Modeling. Preliminary TEM analyses, carried out for several orientations of the sample with respect to the electron beam, show the presence of large ordered areas, indicating a rather well-organized sample. The TEM images recorded in ordered zones correlated with the fcc structure that was suggested also by SAXS but in a mixture with the hcp structure. The value of the lattice parameter is $a_{fcc} = 25$ nm. A typical image recorded along the [111] axis, pointing to sixfold symmetry, is shown in Figure 1.

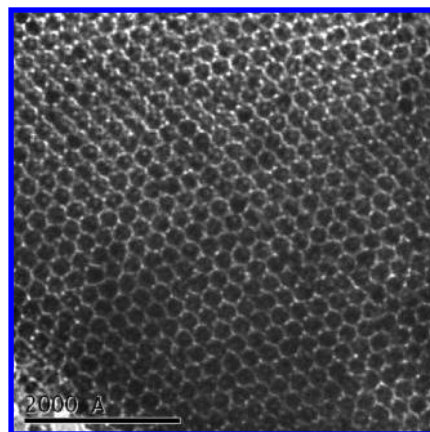**Figure 1.** Bright-field TEM image recorded on an FDU-12 sample along the [111] direction of the fcc lattice.
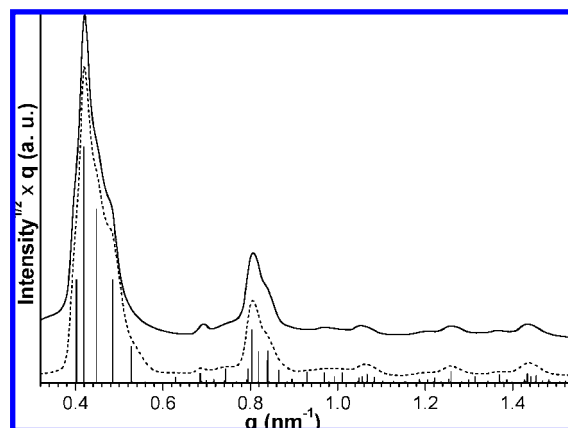

Figure 2. Weighted and Lorentz-corrected observed (solid line) and calculated (dashed line) SAXRD patterns of FDU-12 after CDF−DDM full-profile structure refinement.

The synchrotron SAXRD analysis was done basing on the complex structure of FDU-12 modeled by a mixture of cubic and hexagonal close-packing of spherical cavities. The cavities were arranged in a hexagonal lattice with the trigonal symmetry *P*3. The unit cell was filled by six cavities with positions (0, 0, 0), (1/3, 2/3, 1/6), (2/3, 1/3, 1/3), (0, 0, 1/2), (2/3, 1/3, 2/3), and (1/3, 2/3, 5/6). The profile of the SAXRD pattern was modeled using the Rietveld full-profile formalism.[22] The structural parameters were refined by applying the continuous density function (CDF)[23,24] and the derivative difference minimization (DDM)[25] methods. The selective anisotropic broadening of diffraction peaks due to the structural defects (fcc−hcp intergrowths) was allowed for according to the generalized theory described in a previous paper.[26] As seen in Figure 2, the calculated diffraction profile after CDF−DDM structure refinement reproduces very well the observed one for the following refined structural parameters: lattice constants $a_{trig} = 18.34$ nm, $c = 89.82$ nm; cavity diameter $D = 13.7$ nm; Debye−Waller factor $B = 43.6$ nm^2. The minimal wall thickness ($a_{trig} - D$) reported in Table 1 is in relatively good agreement with the

(18) Thommes, M.; Smarsly, B.; Groenewolt, M.; Ravikovitch, P. I.; Neimark, A. V. *Langmuir* **2006**, *22*, 756–764.

(19) Ehrburger-Dolle, F.; Morfin, I.; Geissler, E.; Bley, F.; Livet, F.; Vix-Guterl, C.; Saadallah, S.; Parmentier, J.; Reda, M.; Patarin, J.; Iliescu, M.; Werckmann, J. *Langmuir* **2003**, *19*, 4303.

(20) Mastronarde, D. N. *J. Struct. Biol.* **1997**, *120*, 343.

(21) Ersen, O.; Hirlimann, C.; Drillon, M.; Werckmann, J.; Tihay, F.; Pham-Huu, C.; Crucifix, C.; Schultz, P. *Solid State Sci.* **2007**, *9*, 1088.

(22) Rietveld, H. M. *J. Appl. Crystallogr.* **1969**, *2*, 65–71.

(23) Solovyov, L. A.; Kirik, S. D.; Shmakov, A. N.; Romannikov, V. N. *Microporous Mesoporous Mater.* **2001**, *44−45*, 17–23.

(24) Solovyov, L. A.; Kirik, S. D.; Shmakov, A. N.; Romannikov, V. N. *Adv. X-Ray Anal.* **2001**, *44*, 110–115.

(25) Solovyov, L. A. *J. Appl. Crystallogr.* **2004**, *37*, 743–749.

(26) Solovyov, L. A. *J. Appl. Crystallogr.* **2000**, *33*, 338–343.

Table 1. Structural and Textural Parameters of the FDU-12 Silica Matrix Determined by SAXRD, 3D-TEM, and Nitrogen Physisorption at 77 K

total pore volume (cm³/g)[a]	cumulative cage mesoporous volume (cm³/g)	spherical cage diameter (nm)[b]	cell parameters (nm)	silica wall thickness (nm)	porosity (%)
0.36	0.27 (5–30 nm)[c]	15 and 11[c]	trigonal[d]	4.6[d]	30[d]
	0.18 (13–17 nm)[c]	13.7[d]	$a = 18.34$	7, 4, 6 (mean value, 6)[e]	22 ± 5[e]
	0.06 (9–13 nm)[c]	12 and 8[e]	$c = 89.82$		
	0.19 (13.7 nm)[d]		cubic face-centered[e]		
			$a = 25$		

[a] Determined for a relative pressure of 0.95. [b] First and second values correspond to the main and "defect" type cage diameters, respectively. [c] Calculated with the NLDFT hybrid kernel method from nitrogen adsorption data. [d] Calculated from SAXRD data. [e] From 3D-TEM.
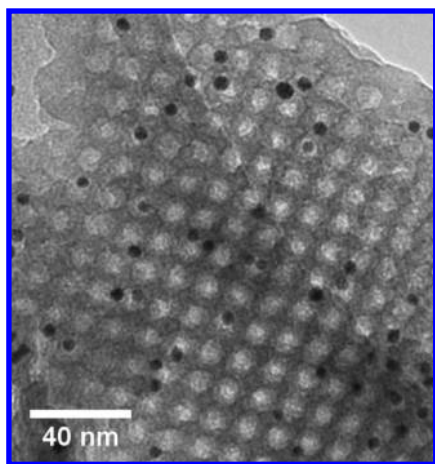

Figure 3. Typical TEM images from the tilt series used to reconstruct the volume of the FDU-12 mesoporous silica, showing the presence of some spherical cages. Dark disks correspond to 10 nm wide gold nanoparticles that are used as fiducial markers in the reconstruction process.

findings from 3D-TEM (see the next section). More detailed analysis (interconnectivity between cavities, etc.) was not feasible due to the defective nature of the structure.

3.2. 3D-TEM Characterization. Although the edge of the analyzed particle is relatively thin, the diameter of the disks observed in Figure 1 cannot be simply related to the size of the spherical cages. Moreover, if the specimen is oriented along a crystallographic axis of the fcc structure, each clear disk is in fact the projection of a column of cavities along this direction. Accordingly, 2D-TEM images average the objects present in the volume of observation and wash out the detailed shape of the cavities and the small connections between them. To recover the detailed morphology and packing of the cavities inside the specimen as well as their 3D connectivity, 3D-TEM experiments were carried out at different magnifications. They allowed us to describe the whole volume of the analyzed sample and thus to get back cross sections along any orientation of the specimen, at the nanometer scale.

An example of a TEM image from the tilt series recorded in bright-field mode and used to reconstruct the volume of the object is given in Figure 3. Three orthogonal cross sections through the reconstructed volume as well as a typical (100) section are shown in Figure 4.

In accordance with previous findings, the ordered area of the structure can be described by the fcc close-packing of spherical cavities each surrounded by 12 nearest neighbors. Taken directly from the reconstruction, the lattice parameter a_{fcc} of the fcc lattice was estimated to be about 25.5 nm and the distance between two neighboring cavities about 18 nm, in good agreement with SAXRD. Note that in SAXRD modeling this distance is equal to the a_{trig} parameter of the trigonal lattice, estimated to be 18.3 nm. Upon analyzing the 3D positions of
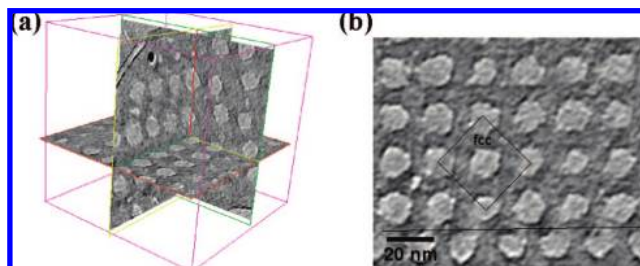

Figure 4. (a) Orthogonal sections through the calculated volume. (b) Typical (100) section showing the arrangement of the cavities and the presence of a stacking defect.

the cavities over a much longer range, we can observe that this structure is rather defective, in agreement with the SAXRD analysis which suggested the presence of stacking faults in the sample. The size of the ordered zones (without any defect) is about 75 nm. Using the exact 3D positions of all the cavities in the reconstructed volume, a direct analysis of the stacking defects in FDU-12 materials is possible as reported hereafter.

3.2.1. Direct Visualization of the Defects. The most commonly observed defect in the FDU-12 sample is the presence of so-called "z-shifted [111] zones". They consist in two rows of cavities shifted along the [111] axis by half of the repeat unit. Three cross sections perpendicular to the [111] axis separated by $d_{111}/2$ are displayed together with 3D views of the cavities' modeling in Figure 5, parts a and b. It may be viewed that the two rows of cavities defining the Q-zone are indeed shifted by $d_{111}/2$ with respect to the cavities belonging to the two neighboring P-zones. Note that such a stacking defect induces a shortening of the distance between cavities at the P–Q interface increasing the probability of interpenetration of the cavities. Therefore, three different wall thicknesses were measured and reported in Table 1. In well-ordered domains (P- and Q-type), the thickness is around 7 nm. Owing to the presence of the translation defects, the wall thicknesses at the P–Q interface are found to be 4 or 6 nm, depending on the relative positions of the cavities. In order to compare the wall thickness with the average value given by SAXRD (4.6 nm, see Table 1), we estimated first the mean density of these translation defects inside the analyzed volume. We observed that, generally, three rows of P-type cavities are followed by two translated rows of Q-type cavities, yielding an average wall thickness of the sample of 6 nm.

Another type of defect observed is the presence of stacking faults along the [111] axis. Projecting the contribution of the cavities (the vacuum parts) to the reconstructed volume onto the same (111) plane (Figure 6a), we observe that all types of sites are occupied by cavities, according to a regular three-layer repeat sequence ABCABC.... The stacking sequence sometimes fails, resulting in stacking faults. A series of successive (111) planes extracted from the reconstruction volume obtained from
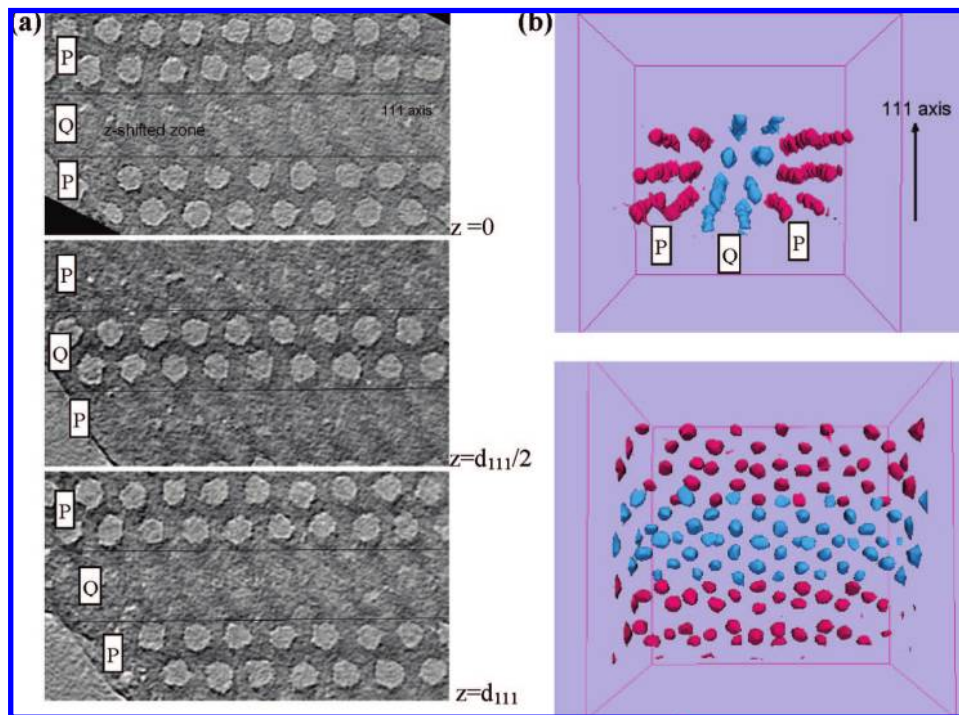
Figure 5. (a) Three (111) sections separated by half of the d_{111} distance. (b) Views of the modeling along $[1 -2 1]$ (up) and $[111]$ (down) axis.
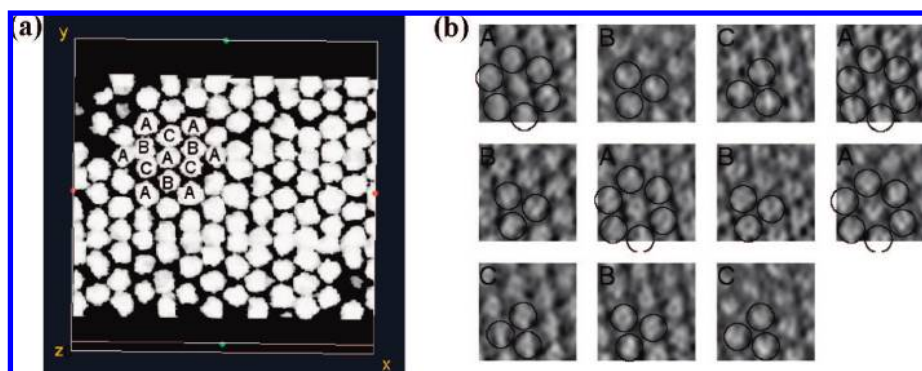

Figure 6. (a) Projection of all cavities onto the same (111) plane: the three types of locations, A, B, and C are occupied by cavities. (b) Successive (111) sections (separated by d_{111}) through the reconstructed volume, showing the presence of stacking faults along the [111] direction.
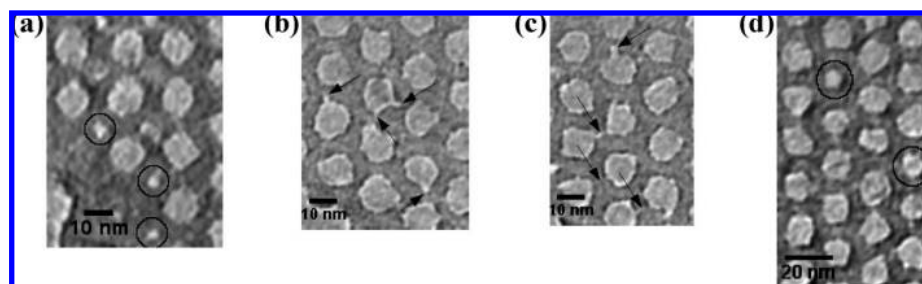

Figure 7. (a) (100) slice showing the presence of a small cavity in an interstitial position in the fcc lattice. (b and c) Two (111) slices revealing the presence of some interconnecting channels. (d) (111) slice that evidences the presence of small well-ordered cavities in the fcc lattice.

a tilt series recorded with a lower magnification in a rather highly defective zone is displayed in Figure 6b. The packing sequence observed, namely, ABCABAB..., provides direct evidence of the presence of stacking faults along the [111] axis.

Beside the stacking defects, we can further observe in some areas of the sample small cavities in interstitial positions in the network defined by the large cavities (Figure 7a). The diameter of these roughly spherical cavities was estimated from the reconstructed volume at about 7 ± 1.5 nm.

3.2.2. Shape of the Cavities and Interconnections. A careful examination of the different sections throughout the reconstructed volume clearly shows that the cavities are only roughly spherical. Approximating the cavities by spheres, their mean diameter was statistically estimated to be about 12 nm, in
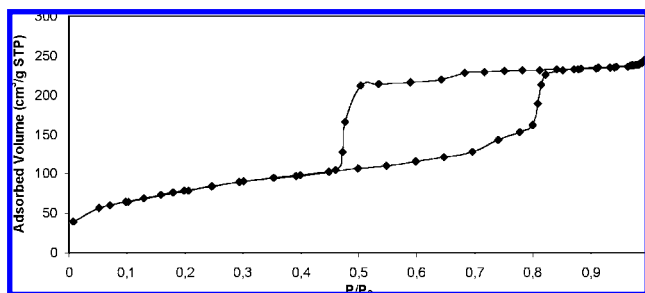
Figure 8. Nitrogen adsorption isotherm at 77 K of FDU-12 silica.

relatively good agreement with SAXS results (13.5 nm, see Table 1). It is worth mentioning that the PSD is quite broad since some smaller cavities are located in the lattice positions (Figure 7d) (mean size of 8 nm), besides interstitial cavities reported above (mean size of 7 nm). Using a segmentation procedure based on gray-level intensities of the voxels and comparing the number of voxels inside cavities to the total volume, we estimated the pore volume fraction to about 22% ± 5%.

For most cavities, protuberances are observed that tend to bridge neighboring cavities with, in some cases, a connection between each other (Figure 7, parts b and c). However, the interconnectivity appears quite random and incomplete, revealing once again the defective character of this material. Since the resolution limit of the 3D-TEM technique estimated in our experimental conditions is about 2 nm, it is difficult to conclude here about the overall connectivity between cavities. The highest diameter (assuming a cylindrical shape) of the connecting pores is around 4 nm.

3.3. Nitrogen Physisorption Study. Nitrogen adsorption performed on the FDU-12 silica sample (Figure 8) is typical of a mesostructured cagelike material with a type IV isotherm and an H2 hysteresis loop. The capillary condensation step (P/P_0 around 0.8) is preceded by a small uptake in the range of P/P_0 of 0.7−0.8, suggesting a bimodal mesopore distribution. The textural and structural parameters are reported in Table 1 together with 3D-TEM and SAXRD modeling results.

The PSD, surface area, and pore volume were calculated from the nonlinear density functional theory (NLDFT) method considering spherical cavities for pores diameters above 5 nm and cylindrical ones below this limit. The fitted isotherm is in good agreement with the experimental one in the whole relative pressure range (results not shown). The PSD reported on Figure 9 shows three types of porosity: a bimodal spherical mesoporosity with a first maximum around 15 nm, a secondary one in the range of 10−12 nm, and a smaller porosity within the range of 2−5 nm with a maximum at 3 nm. The origin and the relevance of these porosities are discussed in the next section.

4. Discussion

The deviation from the ideal $Fm\overline{3}m$ structure in FDU-12 materials was already reported in the literature[4] and related to the presence of a mixture of cubic and hexagonal close-packing structures. This was corroborated by our SAXRD experiments and confirmed by 3D-TEM analysis. Nevertheless, for the first time, a direct visualization of these stacking faults between (111) planes of the structure was achieved. It is thought that the direct visualization of these stacking faults could be very helpful for the design of novel materials using FDU-12 as exotemplate. Moreover, 3D-TEM provided also a direct and unique evidence

for some peculiar stacking defects ("*z*-shifted [111] zones") which have never been reported previously in cagelike meso-structured materials.

The main cavity diameter (15 nm) determined by physisorption is quite close to average values determined by 3D-TEM (12 ± 1.5 nm) and SAXRD (13.7 nm). A simple calculation of the expected pore volume, assuming a defect-free structure with a silica wall density of 2.2 g/cm^3 and spherical cavities of 13.7 nm, deduced from XRD, gives a value of about 0.19 cm^3/g, to be compared to that determined from the NLDFT cumulative pore volume in the range of 13−17 nm (0.18 cm^3/g in Table 1). This means that the majority of the cavities are accessible to the nitrogen probe (the blocked porosity is thus negligible) and that interconnections exist between cavities. This interconnecting porosity could be partially attributed to the smallest porosity observed by nitrogen adsorption study, within the diameter range of 2−5 nm. The existence of this small porosity is corroborated by 3D-TEM, where pore entrances interconnecting spherical cavities are observed (Figure 7, parts b and c), and by the position of the lower closure point of the hysteresis loop (P/P_0 around 0.46). Indeed, for cavity diameter above 4−5 nm, the desorption step is governed by the size of the intrawall porosity that connects the cavity (neck) with the bulk fluid. Since the desorption step occurs at the vicinity of the point of instability of liquid N_2 (P/P_0 close to 0.42−0.48), it means that pore necks have diameters below 4−5 nm and that evaporation occurs then by cavitation.[27,28] Moreover, as shown once again by 3D-TEM (Figure 7, parts b and c), the intrawall connecting porosity is fairly well approximated by a cylindrical shape and its maximum size observed is around 4 nm, in good agreement with the value determined by NLDFT. It also demonstrates the appropriateness of the hybrid DFT model to describe such complex porous structure. Nevertheless, the interconnectivity between cavities evidenced by 3D-TEM appears quite random and incomplete. It could occur that a part of this porosity is not connecting neighboring cavities and/or that supplementary pore entrances with diameter lower than the resolution limit of 3D-TEM technique (here about 2 nm) are present, in accordance with the smallest pore entrances (1.3 nm) reported previously.[4]

The observation of a bimodal distribution of the cavities rather than a broadly dispersed porosity within the range of 10−17 nm (Figure 9) is not fairly explainable. The existence of a secondary porosity (11 nm in diameter) was already observed in a less pronounced manner for the cagelike porous material SBA-16.[29] It could be related to the following.

(i) Cavity pore size heterogeneities within the sample: Since TEM tomography probes only one "crystallite", this hypothesis cannot be excluded. Note that smaller cavities (8 nm in diameter) well located in the fcc lattice were also detected (Figure 7d).

(ii) "Interstitial" defects as shown on Figure 7a: These are only roughly spherical, and therefore the NLDFT result is quite approximate. The value deduced from 3D-TEM experiments (7.0 ± 1.5 nm) is lower than the one observed by NLDFT, but it is likely more realistic.

(iii) Intrawall porosity as evidenced on Figure 7, parts b and c: Calculations with the BJH model, using the adsorption

(27) Ravikovitch, P. I.; Neimark, A. V. *Langmuir* **2002**, *18*, 1550.
(28) Thommes, M.; Smarsly, B.; Groenewolt, P.; Ravikovitch, P. I.; Neimark, A. V. *Langmuir* **2006**, *22*, 756.
(29) Kleitz, F.; Czuryszkiewicz, T.; Solovyov, L. A.; Linden, M. *Chem. Mater.* **2006**, *18*, 5070–5079.
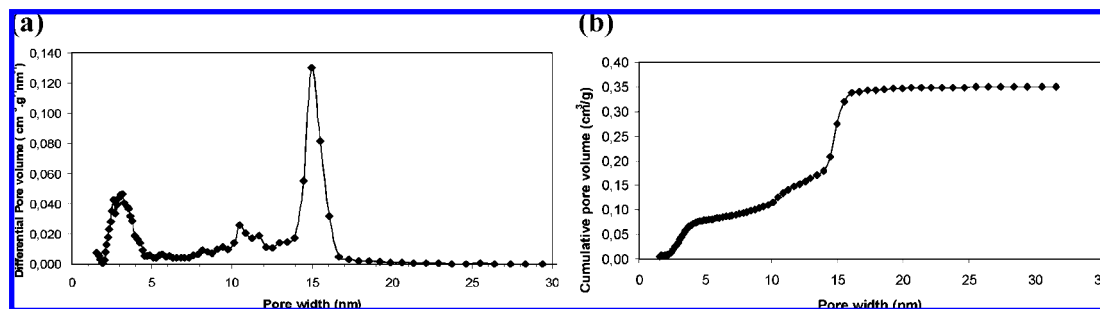
Figure 9. Pore size distribution obtained with the DFT hybrid kernel (a) and corresponding cumulative pore volume (b).

branch and the KJS method[30] and assuming a cylindrical pore shape, were performed to investigate this hypothesis. This yielded also a trimodal cylindrical PSD where the corresponding secondary mesoporosity was in the range of 5−7 nm. Since the maximum size of the connecting pores observed by 3D-TEM is around 4 nm, this hypothesis does not seem to be realistic.

As a result, the secondary mesoporosity (9−13 nm in diameter) is likely to be ascribed to interstitial cavities. They contribute roughly to 0.06 cm^3/g, namely, 20% of the total cavity pore volume (Figure 9b and Table 1), according to the rather high density of these defects in some regions of the sample (Figure 7a).

5. Conclusion

In order to bring new insights to the cagelike ordered mesoporous material FDU-12, we used the ability of electron tomography to provide 3D information which has been validated from nitrogen physisorption and SAXS experiments. Data concerning the structural, textural, and highly defective nature of this phase were extracted. We evidenced here that the fcc structure usually assigned to the FDU-12 materials is in fact an intergrowth of cubic and hexagonal close-packing structures with very limited domains without any defect (in the order of 2−3 close-packed cavities stacking). For the first time, we also provided direct evidence for the presence of peculiar stacking defects between rows of cavities, referred to as "*z*-shifted [111] zones". Their density is high since it concerns two out of five cavity close-packed stacking. Beside these defects, interstitial

(30) Kruk, M.; Jaroniec, M.; Sayari, A. *Langmuir* **1997**, *13*, 6267.

cavities and well-located cavities but with a smaller size were also revealed by this technique, in agreement with the bimodal pore size distribution assessed by physisorption. Moreover, 3D-TEM analysis allowed obtaining reliable estimate for the cage diameter and interconnectivity that were confirmed by SAXRD and physisorption experiments. The individual shapes of the cavities were determined, and the density of the connections, within a resolution limit of about 2 nm, was qualitatively deduced.

Finally, we pointed out that the 3D-TEM technique is an essential tool for multiscale characterization of nanomaterials, providing direct information on the morphology of individual objects and their organization at the nanoscale. In the case of mesoporous materials, it provides essential information on the natures of defects (interstitial cavities, stacking faults, [111]-translated area) and other characteristics of the porosity (pore size distribution, pore volume) that are crucial for understanding the physical−chemical properties and their use in future applications.